

Human Limb Scanning with Improved Accuracy using the *Structure Sensor Pro*TM

Occipital Inc., November, 2021

Abstract

Measurements of the perimeter of 3D meshes reconstructed using the *Pro* version of the *Structure Sensor* present a mean relative error of 0.96%, with a scan-to-scan repeatability of 0.41%. In addition, RMSE measurements as good as 1.30mm have been demonstrated when the *Structure Sensor Pro* is used in combination with its new depth refinement features. In comparison with previous versions of the *Structure Sensor*, the *Pro* version presents, on average, a sensor-to-sensor variability that is at least 5.28 times better, setting this sensor apart as best-in-class for compact and portable scanning applications in which accuracy and repeatability are critical, such as healthcare.

1. INTRODUCTION

Contactless 3D scanning is a well-established technique, having its roots in the scanning of large objects using laser scanners [1-2], having then evolved to the use of compact and mobile devices once techniques were developed capable of optimizing the computational power required for efficient pose estimation, tracking and real-time visualization [3]. That, combined with the development of relatively low-cost 3D scanners, such as the Microsoft *Kinect* and the original *Structure Sensor*, unlocked new applications for the implementation of 3D scanning in mobile devices [4-5].

Occipital is a pioneer in mobile scanning for healthcare applications, having launched the original *Structure Sensor* in 2014, followed by the *Structure Sensor (Mark II)* in 2019, and now followed by the best-in-class *Structure Sensor Pro*. The original *Structure Sensor* disrupted healthcare, replacing significantly more complex and expensive sensors and practices with simple and intuitive operations, thus unlocking expanded use of 3D scanning in medical applications. Notable examples of medical applications that benefit from fast and accurate 3D scanning include the scan of patient body parts for custom-made orthotics and prosthetics (O&P) [6], site characterization for plastic surgery [7], the scanning of wounds in wound care and documentation [8,9], the scanning of patient limbs for monitoring lymphedema [10, 11], and the scanning of patient heads as a replacement to CT-scans for radiotherapy [12], to name a few. Figure 1 illustrates some of those applications with scans captured using the *Structure Sensor*.

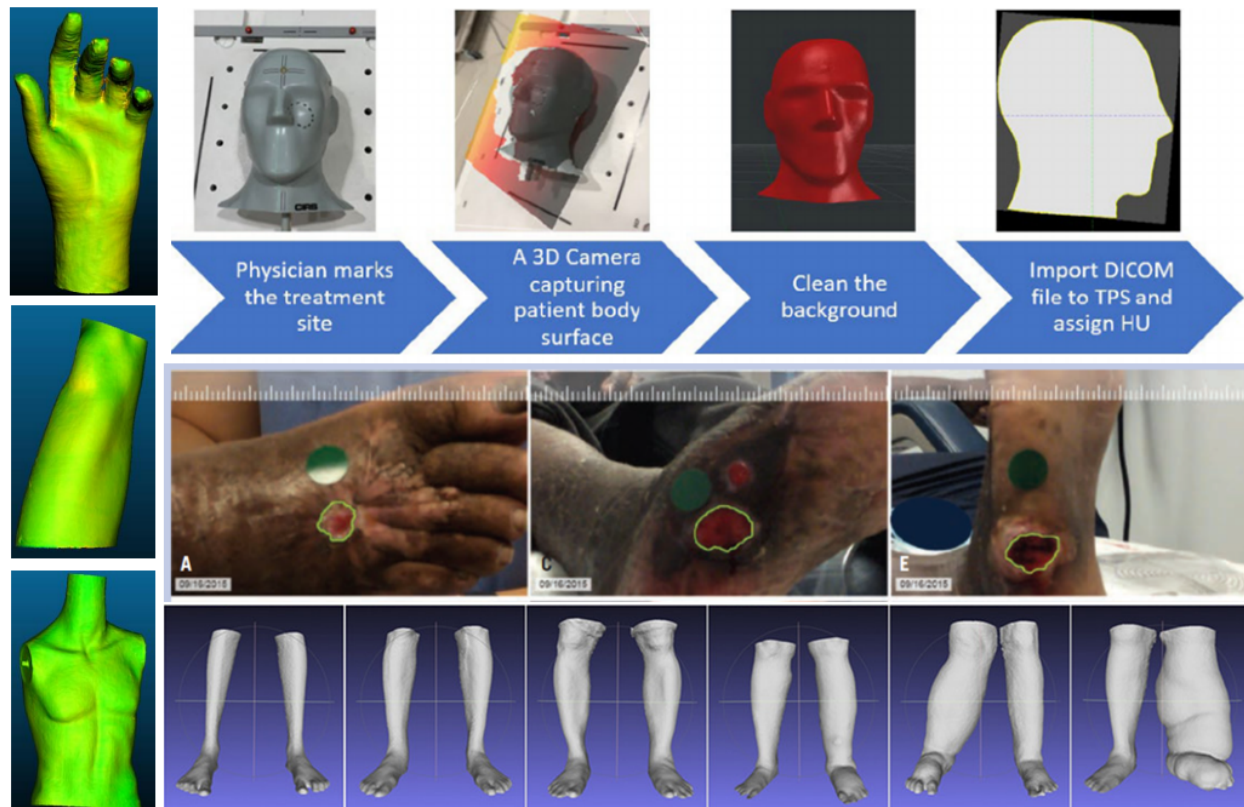


Figure 1: Sample medical applications of the *Structure Sensor*. (Left) Orthopedic scanning for documentation and research (from [6]). (Top) Radiotherapy planning (from [12]). (Middle) Wound measurement and documentation (from [8]). (Bottom) Limb volume and circumference measurement in patients with filarial lymphedema (from [10]).

In the *Structure Sensor Pro*, the *Pro* moniker refers to this sensor’s superior calibration, providing it with improved accuracy and significantly reduced sensor-to-sensor variation. This article describes quantitatively the advantages of the *Pro* sensor in comparison with previous versions of the *Structure Sensor*, in addition to providing a list of settings and recommended methods in order to unlock the full potential of this sensor.

2. METHODS

Given the large number of medical applications of the *Structure Sensor* [6-12] picking a single application becomes a challenge since results from one application are not readily applicable to others. For example, metrics and methods suitable for documenting the shape, depth and color of wounds are not readily suited for reproducing the shape and contact points of foot soles, as required in orthotics. Nevertheless, when reporting quantitative results it is crucial to define the methodology used. As such, we selected the scanning of human limbs as a use-case given its importance to a large number of medical applications, and the possibility to readily extend results obtained in this application to several other adjacent ones, such as head and torso scanning.

Two polyvinyl chloride (PVC) pipes were chosen as phantoms, placed in a room free of obstacles within a 1.5m radius surrounding the pipes. One of the pipes was labeled as *Large* and the other labeled as *Small*, with dimensions of $528.42 \pm 3.19\text{mm}$ in perimeter and $576.26 \pm 2.26\text{mm}$ in length ($358.68 \pm 0.68\text{mm}$, $571.68 \pm 1.68\text{mm}$) for the *Large* (*Small*) pipe, where the errors are plus and minus 3 times the measurement standard deviation, measured a minimum of five times using a calibrated tape measure. In addition, a thin disk of white paper was glued to the top of each pipe, rendering them as solid cylinders instead of hollow pipes. This was done since a solid cylinder is a better representation of a human limb.

Note that cylinders present a special challenge to the object scanning problem: their circular symmetry makes tracking [3] especially challenging. Nevertheless, as results shall demonstrate, the presence of two cylinders in the scene provides the tracking algorithm with sufficient diversity to enable real-time 3D scanning. In addition, besides PVC pipes being easily sourced, allowing results to be easily reproduced, their cylindrical shapes and selected dimensions are representative of those commonly found in human limbs (i.e., legs and arms).

The cylinders were scanned using a total of 89 sensors: 21 *Structure Sensors* (ST01), 36 *Structure Sensor Mark II* (ST02A) and 32 *Structure Sensor Pro* (ST02B). Sensors were selected from a random sampling from Occipital’s inventory.

Cylinders were scanned by the same operator using the iPad 8 iOS device (Apple Corp., Cupertino, CA). Any supported iPad model would be expected to render similar results. Nevertheless, this iPad model was selected for representing the most recent example of a low-end iOS device, one that has been adopted by a large fraction of the user base due to its relatively low cost. Nevertheless, similar results would be expected when using any of the iOS devices supported by the Structure SDK [13].

The application used for performing the scans was the *Scanner* sample iOS application. This application was selected given its widespread availability (it is freely included with the Structure SDK), and the fact that several commercial iOS applications are loosely based on this same application.

2.1. Scanning parameters

Settings of the *Scanner* application were selected to enable direct comparison between different versions of the *Structure Sensor*. They are listed in Table 1.

Table 1: Settings used in the Scanner sample application when capturing experimental scans.

Scanner application setting	Value	Comments
Depth Resolution	VGA	
High Resolution Color	On	
SLAM Option	Default	
	STSLAMManager	

Tracker Type	Depth Only	Tracker settings
	Depth+Visible	
Improved Tracker	On	Mapper settings
High Resolution Mesh	On	
Improved Mapper	On	
Depth Stream Preset	Default	<i>Mark II and Pro versions only</i>
IR Auto Exposure	Off	
IR Manual Exposure	16ms	
IR Analog Gain	2x	

Regarding the choice of SLAM and tracker types, multiple combinations were used in preparatory scans, and the ones listed in Table 1 were selected for presenting the most consistently accurate results. This topic is discussed in more detail in Section 4.

For most applications IR Auto Exposure should be On (in which case IR Manual Exposure is not a selectable choice). However, to prevent ambient IR light from affecting results, we preferred to emphasize the repeatability achieved with a controlled manual exposure of the IR cameras over the flexibility provided by auto exposure. Also, the IR Manual Exposure level was set to maximum (16ms) to maximize the signal-to-noise ratio of the frames captured by the IR cameras. Robustness to motion was not a concern since the objects being scanned are stationary. The same conclusion applies when scanning a cooperative and stationary subject (e.g., a patient standing still).

2.2. Depth map parameters

Structure SDK 1.2, launched simultaneously with the *Structure Sensor Pro*, made available, in beta, two new depth map parameters: *depth search window override* and *depth refinement*. These parameters, exclusive to the *Structure Sensor Pro*, were developed in order to provide that sensor with an additional level of refinement in accuracy. Each one has its own set of tradeoffs, as described next.

Depth search window override allows the reduction of the standard stereo search window, used to calculate the depth map, from the default value (15x11 pixels) to smaller values, as small as 3x3 pixels. In practice, values as small as 7x7 or 9x9 pixels render good results, with smaller values usually resulting in too many gaps in the depth map. A smaller window size presents the advantage of allowing the sensor to scan smaller details, as small as the window size. This results in increased ability to scan, for example between fingers in one's hand, or to more precisely determine the location of edges.

Depth refinement consists of an algorithm that automatically detects edges and removes depth pixels within their vicinity. The result is a depth map with fewer, but higher quality depth pixels. This is

especially useful in applications that require the accurate detection of edges, or of geometric features that depend on the precise detection of edges, such as the calculation of perimeters and volumes.

For clarity, when presenting results we shall distinguish between *Raw* scans (default window size of 15x11 pixels, depth refinement off) and Refined scans, with window sizes clearly defined, and depth refinement on.

2.3. Metrics

Each scan provided us with one point cloud file, saved in the Polygon File Format (PLY). A script written in the Python language was then used to automatically segment individual cylinders from the point cloud and measure their perimeter at different distances from the ground plane (heights). The perimeter measurement was performed by measuring the Euclidean distance between points in the convex hull of the point cloud at a plane parallel to the ground plane, denoted as *heights* (cm). For completeness, the perimeter measurement was repeated at six different heights (10cm, 20cm, 30cm, 40cm, 50cm and 60cm).

To enable a quantitative analysis of results, several metrics were captured from the perimeter measurements, listed in Table 2. The *Slope* metric, in particular, was adopted once we noticed a trend in errors, leading to a linear (positive or negative) slope in the perimeter error for a given sensor. Therefore, a small Slope metric denotes an accurate representation of the geometry of the cylinder.

Table 2: Quantitative metrics extracted from perimeter measurements.

Metric	Units	Explanation
Mean	mm	Mean error, calculated over all perimeter measurements, over all sensors, for a given cylinder.
RMSE	mm	Root-mean square error, calculated over all perimeter measurements, over all sensors, for a given cylinder.
Slope	mm/cm	Slope of perimeter error curve, over all sensors, for a given cylinder.
Var40	mm ²	Variance of error, over all sensors, at the 40cm cylinder height, for a given cylinder.
Sigma	mm	Standard deviation of error, over all sensors, all heights, for a given cylinder.

The *Var40* error metric, on the other hand, was included once we noticed a trend for perimeter error plots to intercept at the 40cm cylinder height. Hence, for a given sensor class, small values of *Slope* and *Var40* metrics indicate good sensor-to-sensor reproducibility.

Finally, the *Sigma* metric was included as representative of the best possible RMSE achievable if measurement bias is accounted for and removed, either by scaling the model or subtracting the bias from perimeter measurements.

3. RESULTS

Figure 2 (left) shows a photo of the two PVC cylinders used as phantoms throughout the study, while Figure 2 (right) shows an example of one of the cylinder reconstructions obtained using the methods described in the previous Section, using a *Structure Sensor Pro*. Different sensors produce meshes that are visually similar, at first inspection. Detailed analysis requires the calculation of perimeter errors, as described next.

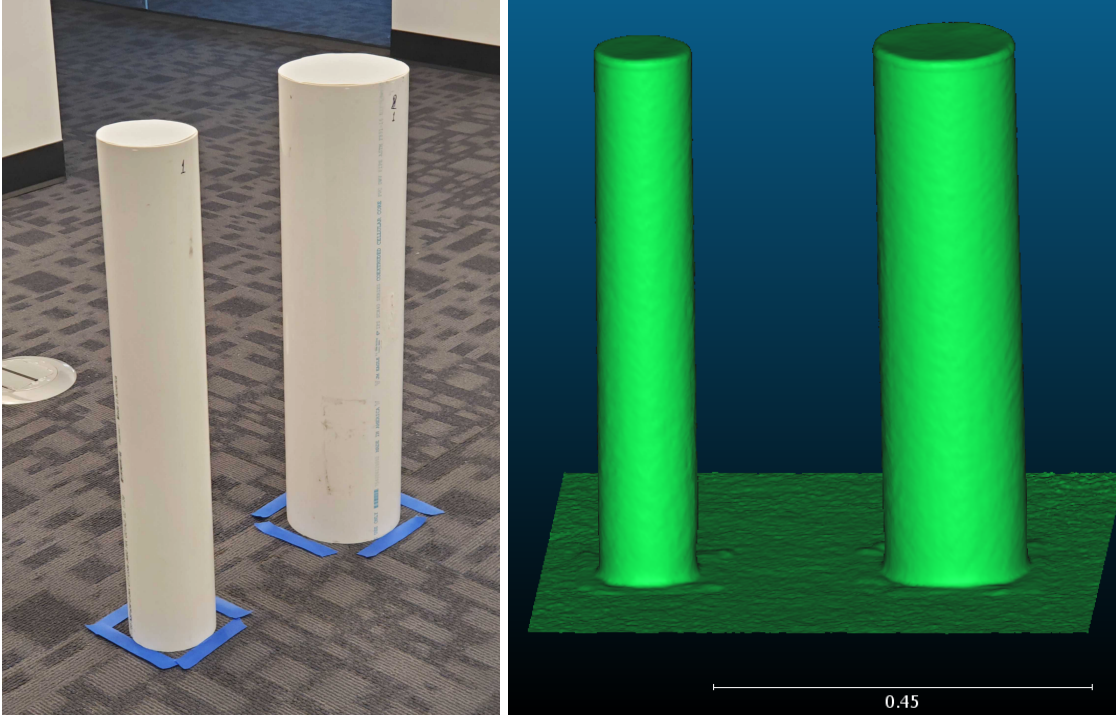


Figure 2: (Left) Photo of two cylinders used during data collection. The *Small* cylinder is on the left and the *Large* cylinder is on the right. (Right) Example of a 3D reconstruction of the same two cylinders, scanned using a *Structure Sensor Pro*.

3.1. Legacy sensors

Figure 3 shows the aggregate cylinder perimeter errors obtained when scanning the same cylinders, using exactly the same settings but different legacy sensors. Each connected line represents a single cylinder scan, each one with a distinct sensor, with 57 sensors total. Different colors are used to help distinguish between different cylinder scans. The Depth-only tracker was used in this case, which presented results slightly better than those obtained using other trackers.

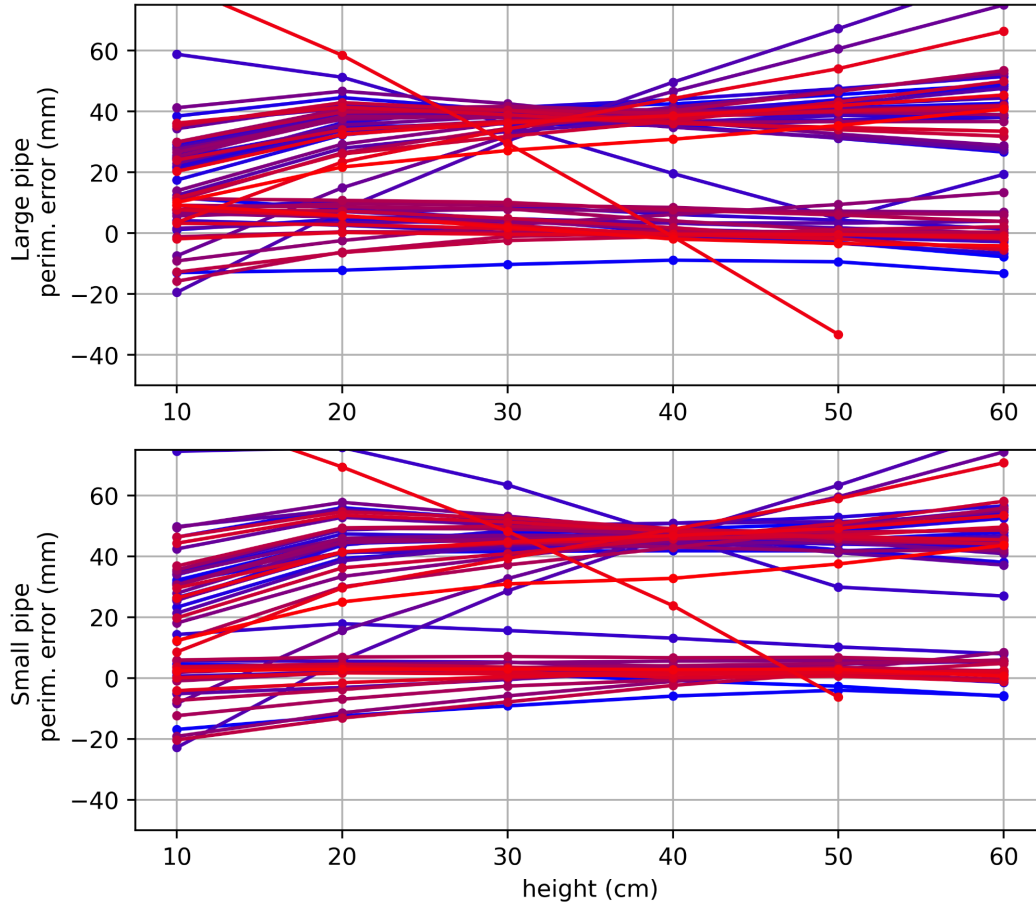


Figure 3: Measured perimeter errors from cylinder scans using distinct legacy sensors. (Top) Errors measured using the *Large* cylinder. (Bottom) Errors measured using the *Small* cylinder. $N = 57$ sensors, Depth-only tracker.

Table 3 summarizes the error metrics. These values become more meaningful later, when compared to those obtained using the *Structure Sensor Pro*. For now, however, note the relatively large Mean, RMSE, Var40 and Sigma errors. Also note that the Slope, while relatively small, is explained by the even prevalence of scans with both positive and negative slopes, some of which can be quite large (-3mm/cm , in the worst case). The significance of those metrics become clearer when compared to those obtained using the *Structure Sensor Pro*.

Table 3: cylinder perimeter error metrics for legacy sensors, Depth-only tracker.

Cylinder	Mean (mm)	RMSE (mm)	Slope (mm/cm)	Var40 (mm ²)	Sigma (mm)
<i>Large</i>	22.79	30.25	0.139	344.9	19.89
<i>Small</i>	27.14	35.72	0.192	465.7	23.21

3.2. *Structure Sensor Pro*, Raw scans

Figure 4, shows the cylinder scan perimeter errors when using 32 distinct *Structure Sensor Pro*, raw scans (default window size, depth refinement off), using the Depth-only tracker and legacy SLAM option of Structure SDK 1.2. Note that, contrary to what was observed when using the legacy sensors under the same conditions, we now have a much more compact distribution of errors. Numeric parameters are presented in Table 4, and the tighter distribution is confirmed by a Var40 parameter of only 6.19mm² (7.05mm²) for the *Large* (*Small*) cylinder, along with a Sigma parameter of 5.80mm (6.37mm) for the *Large* (*Small*) cylinder.

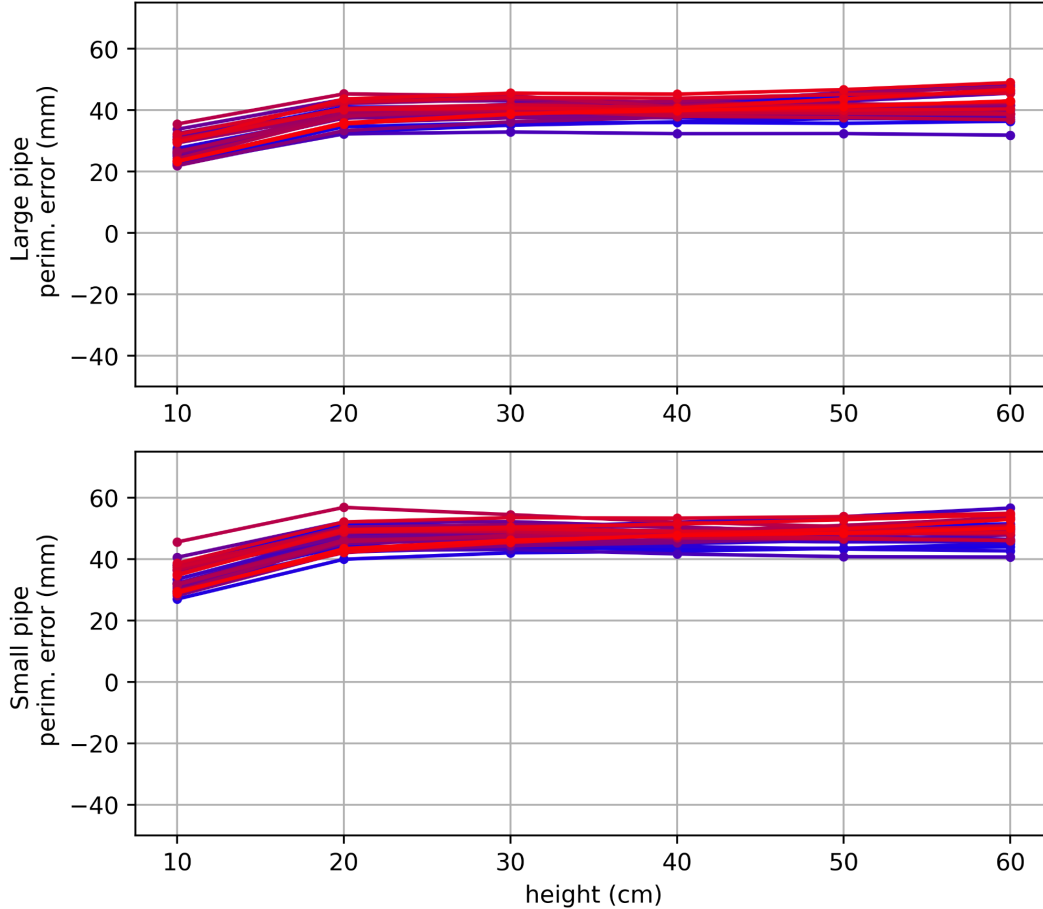


Figure 4: Measured perimeter errors from cylinder scans using distinct *Pro* sensors, raw scans. (Top) Errors measured using the *Large* cylinder, Depth-only tracker. (Bottom) Errors measured using the *Small* cylinder. $N = 32$ sensors.

We also observe a significant offset in the error distribution, as attested by the relatively high Mean error metric: 37.98mm and 45.64mm for the *Large* and *Small* cylinders, respectively. Given these high mean error values, it is no surprise that the RMSE values are also high. The Slope values are slightly higher than those observed with the legacy sensors. In this case, however, the values are meaningful given the consistency of the perimeter error metrics.

Table 4: cylinder perimeter error metrics for *Pro* sensors, raw scans, depth-only tracker.

Cylinder	Mean (mm)	RMSE (mm)	Slope (mm/cm)	Var40 (mm ²)	Sigma (mm)
<i>Large</i>	37.98	38.42	0.217	6.19	5.80
<i>Small</i>	45.64	46.08	0.231	7.05	6.37

Cylinder scans were repeated using the same set of 32 *Pro* sensors, but this time using the Depth+Visible tracker. This tracker, benefiting from the use of the visible camera of the iOS device, in addition to the depth map provided by the sensor, is expected to have a beneficial effect in the reduction of the mean error. Results are shown in Figure 5.

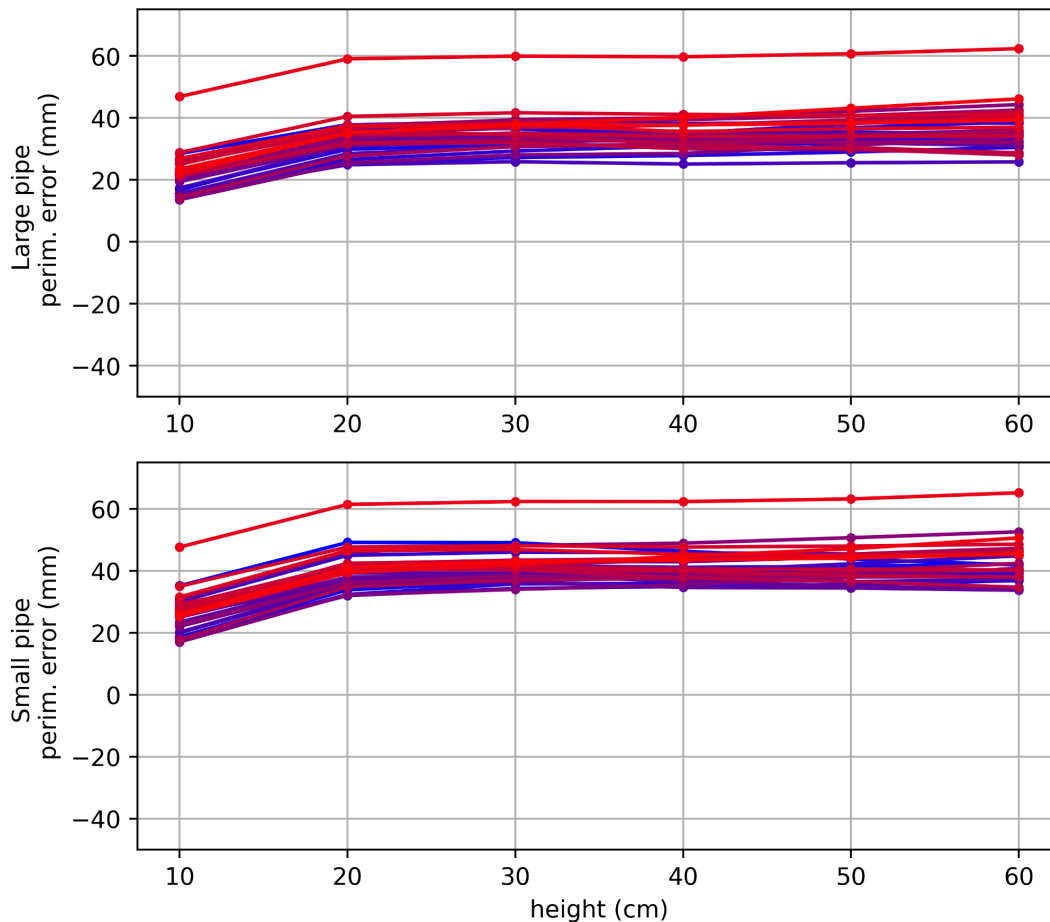


Figure 5: Measured perimeter errors from cylinder scans using distinct *Pro* sensors, raw scans. (Top) Errors measured using the *Large* cylinder, visible+depth tracker. (Bottom) Errors measured using the *Small* cylinder. N = 32 sensors.

Given that all scans are performed using the same iPad, with multiple sensors, sensors had to be attached to the iPad before each scan. This, on its turn, required running the Calibrator application independently for each sensor. Calibrator is one of the free applications made available by Occipital in the Apple Store. It provides an intuitive and user-friendly method allowing end-users to calibrate the extrinsic parameters between the reference IR (infrared) camera in the Structure Sensors and the main visible camera available

on iOS devices. The requirement to re-calibrate extrinsic parameters per sensor, however, resulted in an additional source of variation, leading to a wider spread of the cylinder perimeter error distribution, when compared to those obtained with the Depth-only tracker, which does not depend on the video stream from the visible camera and, thus, is not affected by variations in the extrinsic calibration parameters.

Numeric results are presented in Table 5. As expected, we verify that the error distribution has increased, as attested by the increase in the Var40 and Sigma parameters. This is the case even though the Mean and RMSE metrics have slightly reduced. The Slope parameter, on the other hand, presented little change for either cylinder.

Table 5: Cylinder perimeter error metrics for *Pro* sensors, raw scans, Depth+Visible tracker.

Cylinder	Mean (mm)	RMSE (mm)	Slope (mm/cm)	Var40 (mm²)	Sigma (mm)
<i>Large</i>	32.96	33.87	0.218	33.90	7.81
<i>Small</i>	38.83	39.67	0.250	28.59	8.13

Since Structure SDK 1.1, Occipital started offering another SLAM option for object scanning: STSLAMManager. This new SLAM option also relies on information from the visible camera from the iOS device and, as such, is also sensitive to variations in the extrinsic parameters, but is expected to be able to handle offsets even better than the Depth+Visible tracker in the legacy SLAM. Results are shown in Figure 6, where we see that indeed the mean error of the distribution has been considerably reduced, but at the cost of a large increase in its variance. Note that 4 of the scans rendered meshes so poor that they could not be properly parsed by the metric script. These were dropped from the analysis, resulting in a total of 28 remaining scans.

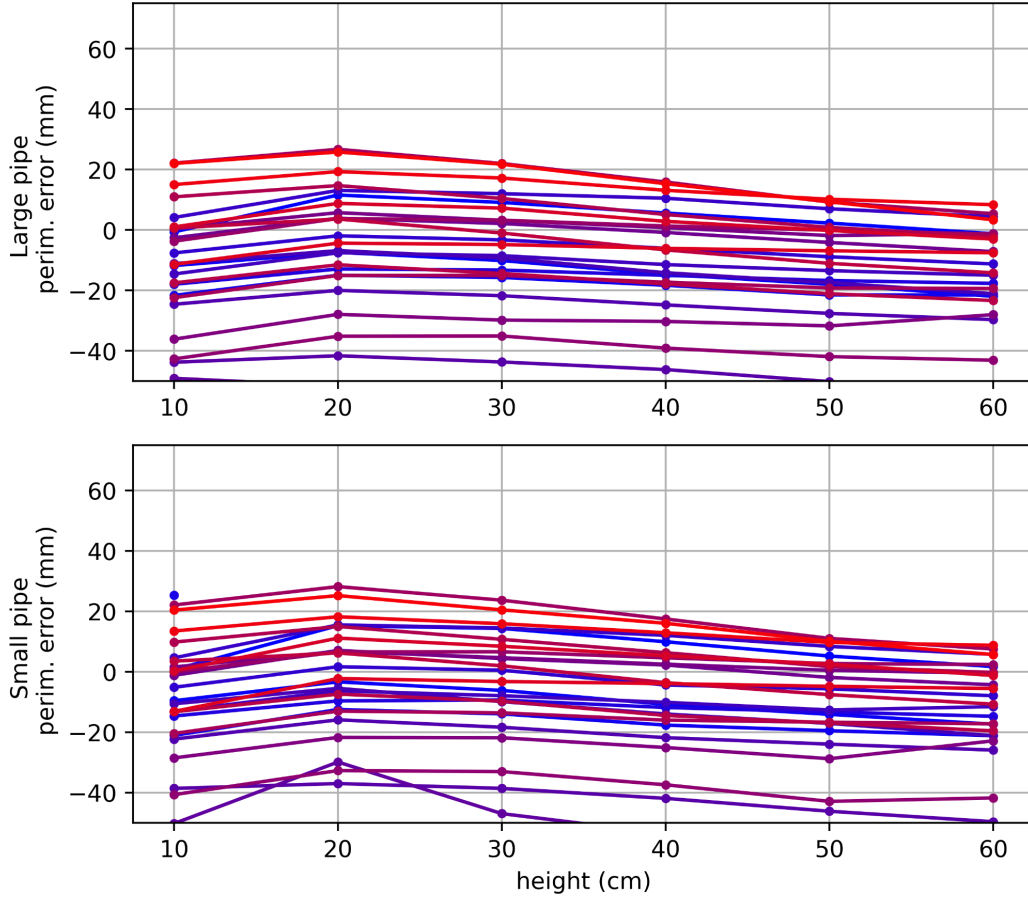


Figure 6: Measured perimeter errors from cylinder scans using distinct *Pro* sensors, raw scans, STSLAMManager. (Top) Errors measured using the *Large* cylinder. (Bottom) Errors measured using the *Small* cylinder. N = 28 sensors.

Table 6 presents the numeric results, confirming that, even though the mean error dropped considerably, the drop was not followed by a drop in the RMSE values. Conversely, the Var40 and Sigma values increased dramatically. The Slopes turned negative, but with an absolute error that is not better than those achieved using other the legacy SLAM configuration.

Table 6: Cylinder perimeter error metrics for *Pro* sensors, raw scans, STSLAMManager.

Cylinder	Mean (mm)	RMSE (mm)	Slope (mm/cm)	Var40 (mm ²)	Sigma (mm)
<i>Large</i>	-4.95	73.75	-0.485	782.3	73.59
<i>Small</i>	-5.83	39.51	-0.146	701.8	39.07

3.3. *Structure Sensor Pro*, refined scans

Given that alternative tracker and SLAM options were not sufficient to simultaneously reduce the bias error while keeping the error distribution in check, we decided to investigate further the root cause of the

bias. This effort led to the development of the new window size override and depth refinement parameters. All results presented in this section were obtained using scans with sensors set to *Depth Refinement On* and a window override size of 9x11 pixels (horizontal x vertical), unless if stated otherwise.

Note that somewhat better results could also be obtained with window sizes as small as 7x7 pixels. However, in some sensors setting such a small search window renders depth maps with a coverage so low as to present a challenge in identifying the ground plane, resulting in the gravity-aligned bounding box becoming unstable. So, 9x11 was determined as a conservative value that, nevertheless, rendered good results.

Figure 7 shows the perimeter errors measured using 12 *Pro* sensors, Depth-only tracker, showing not only a tight distribution of errors but also a significant reduction in the error bias. Numeric results are presented in Table 7, showing a significant drop both in the mean error (7.7mm and 8.00mm for the *Large* and *Small* cylinders, respectively) as well as in the RMSE (8.31mm and 8.93mm, respectively).

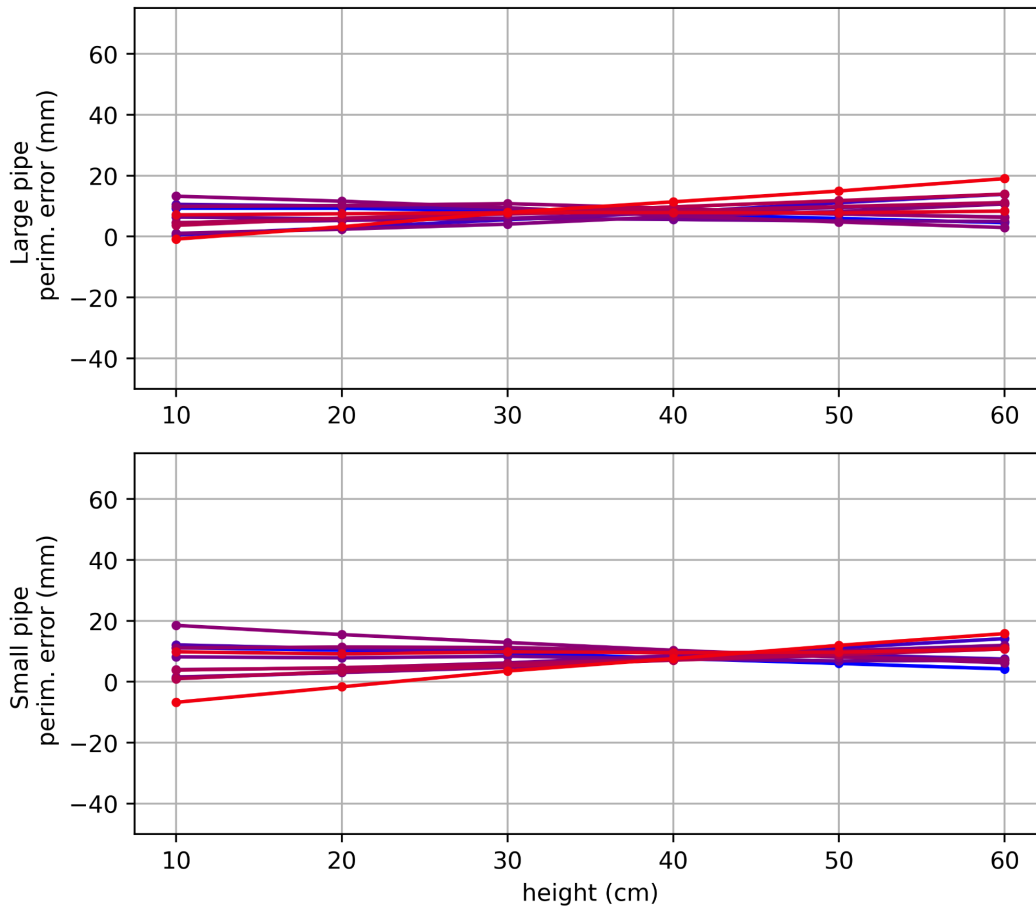


Figure 7: Measured perimeter errors from cylinder scans using distinct *Pro* sensors, refined scans, Depth-only tracker. (Top) Errors measured using the *Large* cylinder. (Bottom) Errors measured using the *Small* cylinder. N = 12 sensors.

Note that the slopes are evenly distributed between positive and negative values, resulting in very small values for the Slope parameter (0.07mm/cm and 0.071mm/cm, respectively). Even the Var40 metric presented a notable reduction, to 2.18mm² and 1.31mm², respectively.

Table 7: Cylinder perimeter error metrics for *Pro* sensors, refined scans, Depth-only tracker.

Cylinder	Mean (mm)	RMSE (mm)	Slope (mm/cm)	Var40 (mm ²)	Sigma (mm)
<i>Large</i>	7.70	8.31	0.070	2.18	3.38
<i>Small</i>	8.00	8.93	0.071	1.31	3.98

3.4. Structure Sensor *Pro*, refined and scaled scans

The relatively small Sigma values (3.38mm and 3.98mm, respectively) suggest the possibility of obtaining a significantly smaller RMSE simply by scaling the model by a fixed factor. A simple search determined that a scale factor of 1.018 was capable of balancing the mean error over all sensors and both cylinders, resulting in the plot shown in Figure 8 and the updated error metrics shown in Table 8.

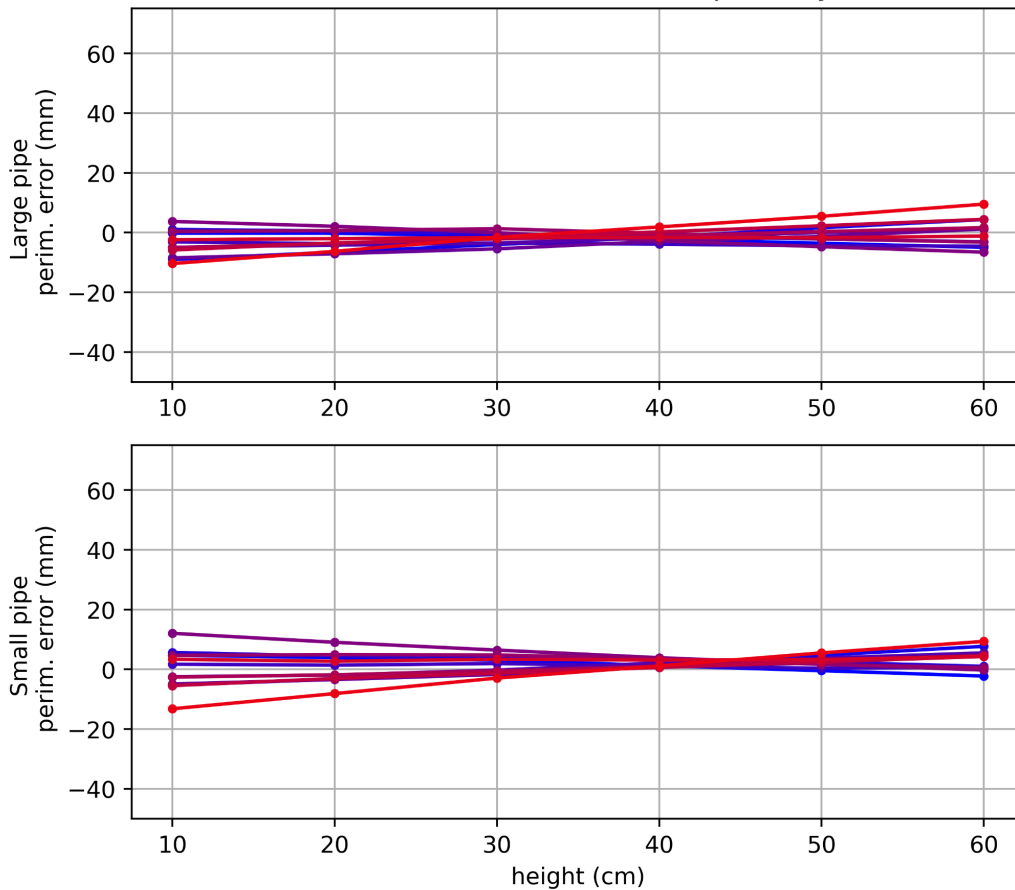


Figure 8: Measured perimeter errors from cylinder scans using distinct *Pro* sensors, refined scans, Depth-only tracker, with a scale factor of 1.018 applied to the reconstructed mesh. (Top) Errors measured using the *Large* cylinder. (Bottom) Errors measured using the *Small* cylinder. N = 12 sensors.

Scaling the reproduced mesh by 1.018 results in making it slightly larger. Consequently, the perimeter errors shift downwards but do not change shape. This results in significant reduction in the Mean error metrics (balanced to -1.81mm and 1.54mm between the *Large* and *Small* cylinders), and a corresponding reduction in the RMSE (3.84mm and 4.26mm, respectively). This is equivalent to a residual fractional error of 0.73% (1.19%) over the total perimeter of the *Large* (*Small*) cylinder, resulting in an averaged relative error of 0.959%.

Table 8: Cylinder perimeter error metrics for *Pro* sensors, refined scans, with a correction factor of 1.018.

Cylinder	Mean (mm)	RMSE (mm)	Slope (mm/cm)	Var40 (mm ²)	Sigma (mm)
<i>Large</i>	-1.81	3.84	0.070	2.18	3.38
<i>Small</i>	1.54	4.26	0.071	1.31	3.98

Note that the Slope, Var40 and Sigma error factors were not affected by the scale change, as expected.

4. DISCUSSION

Numeric results demonstrate, beyond a doubt, that the *Structure Sensor Pro* provides significant accuracy improvements in the measurement of perimeters of objects with dimensions equivalent to those of human limbs, when compared to results obtained using legacy sensors.

If we are to select a single perimeter metric for comparison, the standard deviation (Sigma) over multiple heights is the most interesting one given the fact that smaller Sigma values are unequivocally associated with reduced errors, and no further error reduction is possible, even after applying an aggregate scaling factor over multiple sensors. As such, using the averaged Sigma between *Large* and *Small* cylinders as a single error metric, we can produce Table 10 comparing all results over multiple sensors, multiple trackers.

Table 10: Comparison of Sigma values, averaged across cylinders.

Sensor Condition	Tracker	Averaged Sigma (mm)	Comparison to <i>best result</i> *
Legacy	Depth-only	21.55	5.85
	Depth+Visible	19.42	5.28
	STSLAMManager	101.4	27.55
	Depth-only	6.09	1.65

<i>Pro</i> , Raw	Depth+Visible	7.97	2.17
	STSLAMManager	56.33	15.3
<i>Pro</i> , Refined	Depth-only	3.68	1*
	Depth+Visible	9.99	2.71
	STSLAMManager	230.4	16.0

* *Best result* corresponds to the result with the lowest averaged RMSE. Namely, using the *Structure Sensor Pro* with a refined depth map and the Depth-only tracker. Other settings are described in Table 1.

Table 10 makes it clear that the best possible results are obtained using the *Structure Sensor Pro* with depth refinements (Depth Refinement On, window size of 9x11) using the Depth-only tracker, resulting in an averaged Sigma of 3.68mm. Taking the ratio between that value and all the Sigma values obtained under all other conditions we end up with the rightmost column in table 10, allowing us to conclude that the *Structure Sensor Pro*, with refined depth, provides us with results that are, on average, at least 5.28 times better than those obtained using legacy sensors, using the Depth+Visible tracker, which provided results slightly better than those obtained using the Depth-Only tracker for those sensors.

4.1. Repeatability of the *Structure Sensor Pro*

Section 3.4 demonstrated that the lower sensor-to-sensor variability provided by the *Structure Sensor Pro* allows one to effectively take the aggregate bias into account and further reduce the perimeter measurement error. In this Section we will explore what is possible when using the same sensor to scan the same pair of objects (cylinders) multiple times. In other words, we will report on the repeatability of the *Structure Sensor Pro*.

Figure 10 shows the result obtained when the same *Pro* sensor was used 12 times, by the same operator, to perform 12 distinct scans (the sensor was used to perform other scans between each one of the 12 scans, with an average time interval of about 25 minutes between each scan).

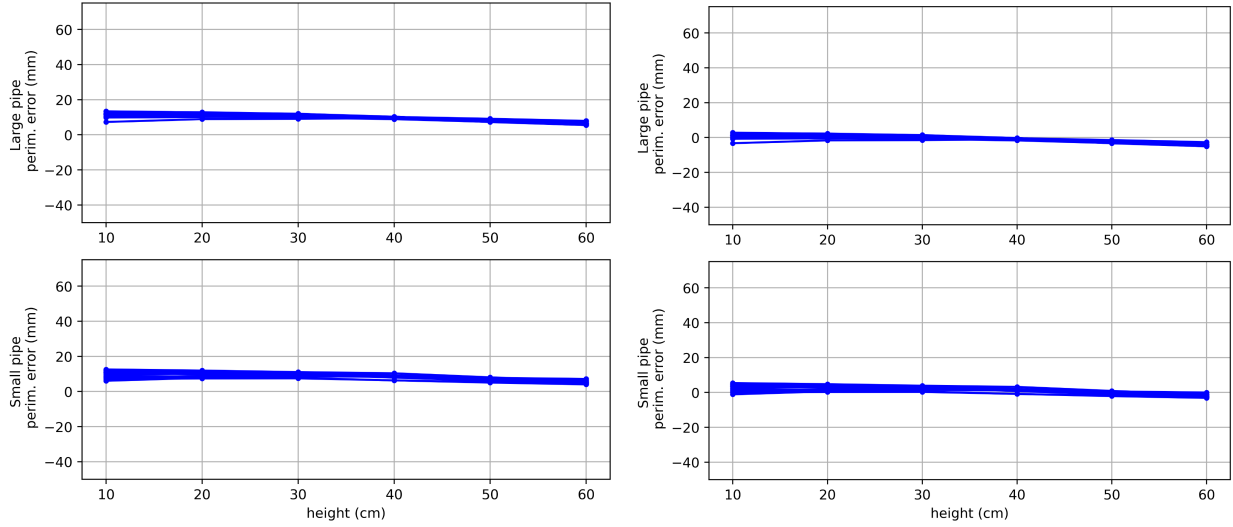


Figure 10: Measured perimeter errors from cylinder scans using the same *Pro* sensor 12 times, refined scans, Depth-only tracker. (Top) Errors measured using the *Large* cylinder. (Bottom) Errors measured using the *Small* cylinder. (Left) no scale factor. (Right) Scale factor of 1.02.

Following best practices, the Depth-only tracker was used, in addition to depth refinement and reduced window sizes (9x11). The plots on the left show results obtained without scaling, resulting in a bias (mean error) of 9.88mm (8.56mm) for the *Large* (*Small*) cylinder. The plots on the right show the same result after applying a scale factor of 1.02, optimized for this sensor. This allows us to balance the bias between cylinders, resulting in a residual bias of -0.92mm (1.10mm) for the *Large* (*Small*) cylinder, as shown in Table 11.

Table 11: Repeatability - cylinder perimeter error metrics for a *Pro* sensor used multiple times (refined scans, 1.02 scale factor, Depth-only tracker).

Cylinder	Mean (mm)	RMSE (mm)	Slope (mm/cm)	Var40 (mm ²)	Sigma (mm)
<i>Large</i>	-0.92	2.33	-0.11	0.20	2.14
<i>Small</i>	1.10	2.47	-0.10	1.18	2.21

Table 11 also shows that the Var40 error is only 0.20mm² (1.18mm²) for the *Large* (*Small*) cylinder, while their Sigma values are only 2.14mm and 2.21mm, respectively. Taking their corresponding perimeters into account, that corresponds to relative errors of 0.405% and 0.616%, respectively. Note that the Var40 and Sigma values are not affected by the scaling factor. Sigma, in particular, is representative of the repeatability that should be expected of this sensor. The residual RMSE is slightly larger than the Sigma values, given the goal to split the difference between means. They are 2.33mm and 2.47mm for the *Large* and *Small* cylinder, corresponding fractional errors of 0.441% and 0.689%, respectively.

4.2. Depth refinements effect on mesh RMSE

Figure 11 helps explain why depth refinements result in such a significant reduction in RMSE. The plots show the histogram of distances (errors) in all points available in the point cloud when measured with respect to a reference model built according to the measured cylinder dimensions. The measurement and plots were obtained using the CloudCompare open-source software application [14].

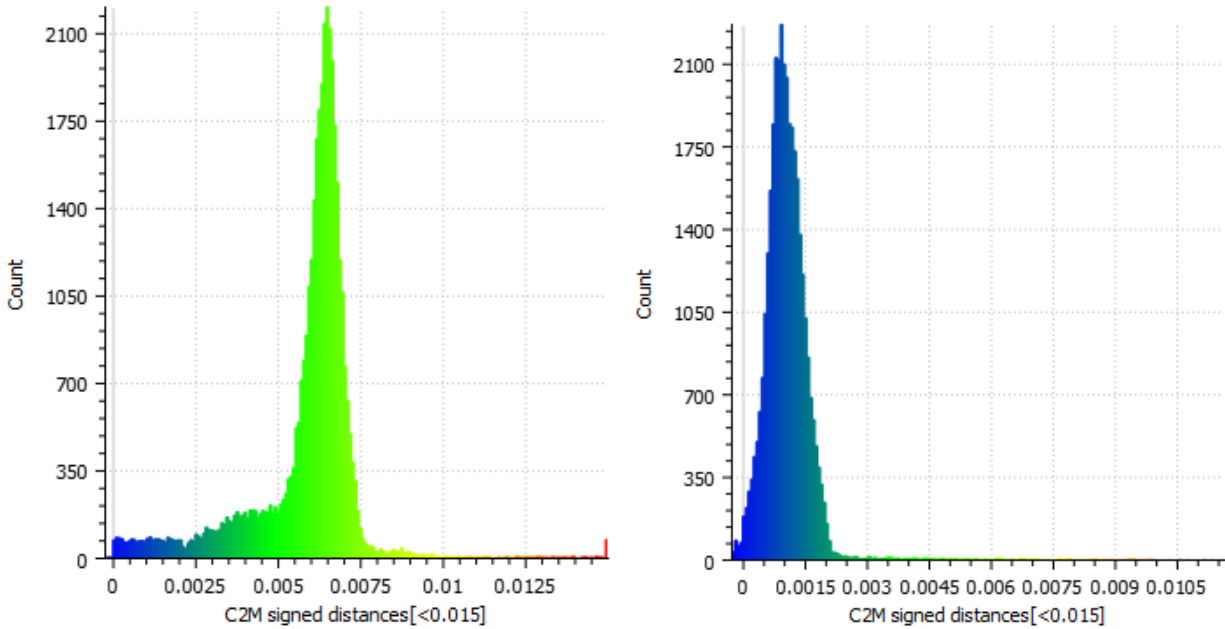


Figure 11: Example of reconstruction errors using the Structure Sensor Pro, Large cylinder. Left - Raw scan. Right - Refined scan, showing significantly lower bias and somewhat smaller variance.

The histogram on the left corresponds to a cylinder scan using a *Structure Sensor Pro*, Depth-only tracker, raw depth scan (no refinements), resulting in a tight distribution but with significant bias. The histogram on the right corresponds to another scan captured using the same sensor, same tracker, but with depth refinements on (9x9 window size), resulting in a) a significant reduction in bias (from 5.87mm to 1.08mm), and b) a reduction in standard deviation (from 1.71mm to 0.73mm), resulting in a significant reduction in RMSE, from 6.11mm to 1.30mm. This result demonstrates the simple fact that rejecting the less accurate points in the depth map results in higher accuracy in the final mesh reconstruction.

Note that the resulting “holes” in the refined depth map are quickly filled by other points in the depth map as the user moves the sensor during the scanning process. Therefore, the tradeoff of *fewer pixels* for *better quality pixels* is a favorable one, with no significant drawbacks. Also note that it is fairly easy to demonstrate impressive RMSE values when dealing with low-resolution meshes with a relatively small number of faces. This is not the case here: both meshes (raw and refined) retain a large number of faces, totaling 79,395 and 70,268 faces, respectively.

5. CONCLUSION

This work has demonstrated that the *Structure Sensor Pro*, when used in combination with the Structure SDK, is an accurate instrument for measuring perimeters of objects comparable to human limbs. This fact, combined with its portability and ease of use, render it as a *best in class* metrology tool for many healthcare applications that benefit from personalized care. These include custom orthotics and prosthetics, custom compression garments used in the treatment of lymphedema, wound documentation and the replacement of CT-scans for radiotherapy.

Numeric results demonstrate that the *Structure Sensor Pro* is at least 5.28 times better than legacy sensors when measuring perimeters. We have shown perimeter measurement RMSE results as good as 0.44% relative to the total perimeter, repeatability results as good as 0.41%, and mesh RMSE results as good as 1.30mm, with more than 70k faces. Furthermore, results confirm that most accurate results are obtained when using the Depth-only tracker available in the Structure SDK, combined with the new window size override and depth refinement parameters made available since the Structure SDK 1.2.

6. REFERENCES

- [1] Curless, B., & Levoy, M. (1996). A volumetric method for building complex models from range images. Proceedings of the 23rd Annual Conference on Computer Graphics and Interactive Techniques, SIGGRAPH 1996, 303–312. <https://doi.org/10.1145/237170.237269>
- [2] Levoy, M., Rusinkiewicz, S., Ginzton, M., Ginsberg, J., Pulli, K., Koller, D., Anderson, S., Shade, J., Curless, B., Pereira, L., Davis, J., & Fulk, D. (2000). The digital Michelangelo project: 3D scanning of large statues. Proceedings of the ACM SIGGRAPH Conference on Computer Graphics.
- [3] Klein, G., & Murray, D. (2007). Parallel Tracking and Mapping for Small AR Workspaces. 2007 6th IEEE and ACM International Symposium on Mixed and Augmented Reality, 225–234. <https://doi.org/10.1109/ISMAR.2007.4538852>
- [4] Newcombe, R. A., Izadi, S., Hilliges, O., Molyneaux, D., Kim, D., Davison, A. J., Kohli, P., Shotton, J., Hodges, S., & Fitzgibbon, A. (2011). KinectFusion: Real-time dense surface mapping and tracking. 2011 10th IEEE International Symposium on Mixed and Augmented Reality, ISMAR 2011. <https://doi.org/10.1109/ISMAR.2011.6092378>
- [5] Izadi, S., Kim, D., Hilliges, O., Molyneaux, D., Newcombe, R., Kohli, P., Shotton, J., Hodges, S., Freeman, D., Davison, A., & Fitzgibbon, A. (2011). KinectFusion: Real-time 3D reconstruction and interaction using a moving depth camera. UIST'11 - Proceedings of the 24th Annual ACM Symposium on User Interface Software and Technology. <https://doi.org/10.1145/2047196.2047270>
- [6] Redaelli, D. F., Gonizzi Barsanti, S., Fraschini, P., Biffi, E., & Colombo, G. (2018). Low-cost 3D devices and laser scanners comparison for the application in orthopedic centres. International Archives of the Photogrammetry, Remote Sensing and Spatial Information Sciences - ISPRS Archives, 42(2), 953–960. <https://doi.org/10.5194/isprs-archives-XLII-2-953-2018>

- [7] Oranges, C. M., Madduri, S., Brantner, P., Msallem, B., Giordano, S., Benitez, B., Kalbermatten, D. F., Schaefer, D. J., & Thieringer, F. M. (2019). Three-dimensional Assessment of the Breast: Validation of a novel, simple and inexpensive scanning process. *In Vivo*, 33(3), 839–842. <https://doi.org/10.21873/invivo.11548>
- [8] Anghel, E. L., Kumar, A., Bigham, T. E., Maselli, K. M., Steinberg, J. S., Evans, K. K., Kim, P. J., & Attinger, C. E. (2016). The Reliability of a Novel Mobile 3-dimensional Wound Measurement Device. *Wounds : A Compendium of Clinical Research and Practice*, 28(11), 379–386. <http://europepmc.org/abstract/MED/27589359>
- [9] Chan, K. S., Chan, Y. M., Tan, A. H. M., Liang, S., Cho, Y. T., Hong, Q., Yong, E., Chong, L. R. C., Zhang, L., Tan, G. W. L., Chandrasekar, S., & Lo, Z. J. (2021). Clinical validation of an artificial intelligence-enabled wound imaging mobile application in diabetic foot ulcers. *In International Wound Journal*. <https://doi.org/10.1111/iwj.13603>
- [10] Yahathugoda, C., Weiler, M. J., Rao, R., De Silva, L., Dixon, J. B., Weerasooriya, M. V., Weil, G. J., & Budge, P. J. (2017). Use of a Novel Portable Three-Dimensional Imaging System to Measure Limb Volume and Circumference in Patients with Filarial Lymphedema. *The American Journal of Tropical Medicine and Hygiene*, 97(6), 1836–1842. <https://doi.org/10.4269/ajtmh.17-0504>
- [11] Binkley, J. M., Weiler, M. J., Frank, N., Bober, L., Dixon, J. B., & Stratford, P. W. (2020). Assessing Arm Volume in People During and After Treatment for Breast Cancer: Reliability and Convergent Validity of the LymphaTech System. *Physical Therapy*, 100(3), 457–467. <https://doi.org/10.1093/ptj/pzz175>
- [12] Skinner, L., Knopp, R., Wang, Y. C., Dubrowski, P., Bush, K. K., Limmer, A., Trakul, N., Million, L., Marquez, C. M., & Yu, A. S. (2021). CT-less electron radiotherapy simulation and planning with a consumer 3D camera. *Journal of Applied Clinical Medical Physics*, 22(7), 128–136. <https://doi.org/10.1002/acm2.13283>
- [13] Structure SDK Developer Portal: <https://developer.structure.io/sdk>
- [14] CloudCompare project: <http://www.cloudcompare.org/>